Final Report

In-Flight Flow Visualization Using Infrared Thermography

by

C.P. van Dam and H.J. Shiu
Department of Mechanical and Aeronautical Engineering
University of California, Davis
One Shields Avenue
Davis, CA 95616

to

D.W. Banks
Mail Stop D-2033
NASA Dryden Flight Research Center
Edwards, CA 93523

NASA NCC4-108

November 1997

Abstract

The feasibility of remote infrared thermography of aircraft surfaces during flight to visualize the extent of laminar flow on a target aircraft has been examined. In general, it was determined that such thermograms can be taken successfully using an existing airplane/thermography system (NASA Dryden's F-18 with infrared imaging pod) and that the transition pattern and, thus, the extent of laminar flow can be extracted from these thermograms. Depending on the in-flight distance between the F-18 and the target aircraft, the thermograms can have a spatial resolution of as little as 0.1 inches. The field of view provided by the present remote system is superior to that of prior stationary infrared thermography systems mounted in the fuselage or vertical tail of a subject aircraft. An additional advantage of the present experimental technique is that the target aircraft requires no or minimal modifications.

An image processing procedure was developed which improves the signal-to-noise ratio of the thermograms. Problems encountered during the analog recording of the thermograms (banding of video images) made it impossible to evaluate the adequacy of the present imaging system and image processing procedure to detect transition on untreated metal surfaces. The high reflectance, high thermal difussivity, and low emittance of metal surfaces tend to degrade the images to an extent that it is very difficult to extract transition information from them. The application of a thin (0.005 inches) self-adhesive insulating film to the surface is shown to solve this problem satisfactorily. In addition to the problem of infrared based transition detection on untreated metal surfaces, future flight tests will also concentrate on the visualization of other flow phenomena such as flow separation and reattachment.

Nomenclature

c	wing chord
C_L	lift coefficient
h	altitude
KCAS	calibrated airspeed in knots
M_∞	freestream Mach number
r	leading edge radius
R_{bar}	attachment line Reynolds number
Re	Reynolds number based on c and V_∞
S	wing planform area
T_{t_∞}	total temperature of flow
T_W	wall temperature
V_∞	freestream velocity
W	aircraft weight
W_∞	spanwise component of freestream velocity
x	distance along the chord
Λ	leading-edge sweep angle
ν	kinematic viscosity

Introduction

In recent years interest has continued in the development of low-drag airplanes with extended runs of laminar flow. This interest has resulted in the demand for wind-tunnel and flight experiments to investigate the extent of laminar flow on wings and bodies and the sensitivity of the laminar flow to manufacturing tolerances and surface contamination. Recently, a greater awareness developed for the effects of laminar flow on the high-angle-of-attack characteristics of maneuverable military aircraft as well as on the high-lift characteristics of transport aircraft. Flow separation at these conditions is related to the extent of laminar flow and, thus, to the phenomenon of laminar-turbulent transition. To better predict the aerodynamic forces generated by aircraft at high-angle-of-attack and/or high-lift conditions, an improved understanding of the transition phenomena at full-scale flight conditions is required.

A large number of techniques is available to study boundary-layer transition on aircraft surfaces including sublimating chemicals[1], oil flow[2], liquid crystals[3], luminescent temperature-sensitive paints[4], surface oil film interferometry[5], hot-film anemometry[3,6], thermocouples[3], microphones[7], total pressure (Preston) tubes[8], infrared thermography[2,3,6], etc.

Several of these transition-detection techniques are intrusive; i.e., they affect the development of the laminar boundary layer and, thus, transition. Devices such as thin hot films, thermocouples, and microphones provide excellent quantitative information on transition. However, the information is strictly local and many tightly spaced hot films, thermocouples or microphones are required to obtain sufficient global information. Techniques such as sublimating chemicals and oil flow remain very popular for transition measurement in ground-based facilities. Unfortunately only one condition per surface application can be tested and this limitation makes these techniques less desirable for flight experimentation. Recently, techniques based on surface application of liquid crystals and luminescent temperature-sensitive paints have received more attention. These techniques require more-or-less permanent surface treatment, something that may be less desirable, as well as a significant amount of preparation and calibration time. Also, some of these materials are considered to be hazardous and, thus, require special pre- and post-flight procedures for application and removal. As a result of these insufficiencies and drawbacks, infrared thermography is often the preferred technique to study transition because it (1) is nonintrusive, (2) provides global information, (3) is reversible, and (4) requires no or minimal treatment of the surface in the subject area.

In the following section, the principles of infrared thermography for in-flight transition detection are explained in detail. Next, the image processing procedure that has been developed to obtain high quality digital images depicting the surface temperature differences (thermograms) is explained. This procedure has been used to analyze infrared images from NASA Dryden's T-34C and NASA Langley's B737-100; the results for the former are presented and discussed in the following section. In the last section of this report, some recommended flight experiments and future developments are discussed.

In-Flight Infrared Flow Visualization

Infrared thermography is based on the fact that the boundary-layer state affects the temperature differences that can exist between the surface and the flow. At low Mach numbers ($M_\infty << 1$) a temperature difference can be created between the flow and the surface by cooling or heating the flow or by cooling or heating the surface. In ground-based facilities one may have control over the temperature of the flow; however, this is impractical in flight experiments. Several techniques are available to heat or cool the surface. Horstmann et al.[9] utilized a heating sheet to raise the surface

temperature. Unfortunately this is only practical when a glove is used to raise the test surface and to provide space for the instrumentation including a surface heater. A small temperature difference between the aircraft surface and the fluid can also be obtained by solar radiation of the aircraft surface, or by a change in flight altitude utilizing the atmospheric temperature gradient. The heat transfer due to convection depends on the difference between the wall temperature and the total temperature of the flow as well as the wall shear stress. At a given location along the surface, the laminar boundary layer will generate a lower shear stress than a turbulent boundary layer and, consequently, the laminar heat flux will be lower than the turbulent heat flux. This will cause the laminar surface to be slightly warmer than the turbulent surface if $T_w > T_{t_\infty}$ (where T_w is the wall temperature and T_{t_∞} is the total temperature of the flow) and slightly cooler if $T_w < T_{t_\infty}$. This surface temperature difference is especially noticeable at transition and it is this difference that is measured by the infrared imager.

At higher Mach numbers, a temperature difference between the surface and the flow is created (without surface heating or cooling) as a result of a temperature recovery factor in the boundary layer which is less than unity. This causes the wall temperature to be less than the total temperature of the undisturbed flow, $T_w < T_{t_\infty}$. The recovery factor is dependent on the boundary-layer state with laminar flow having a slightly lower value than turbulent flow. This will cause the laminar surface to be slightly cooler than the turbulent surface.

Note that in addition to heat flux due to convection, solar radiation, etc., there may also be thermal conductance within the aircraft surface. Especially lateral heat conduction within a metal aircraft skin will cause flattening of the temperature gradients in the transition region and may make transition detection using infrared thermography virtually impossible.

This brings us to problems with infrared thermography for in-flight transition detection. First, a problem exists with thermal heat conductance encountered with metal structures. This problem can be solved by applying a thin plastic film with a low thermal conductance. In previous flight experiments, thin sheets of self-adhesive vinyl were applied to the wing and this solved the heat conductivity problem without affecting the development of the laminar boundary layer. By using black vinyl, the solar absorptance of the surface and, consequently, the temperature difference between the wall and the flow was also significantly enhanced.[10] For instance, the solar absorptance for black plastic is 0.94 whereas the same material in white has a value of 0.39.[11] These self-adhesive vinyl sheets are easily applied and removed without causing damage to the existing surface coating.

Second, there are also problems involving limited field of view. Although this is less of a problem for larger transport aircraft with windows a significant distance above the wing[6], it is a significant problem for smaller light aircraft [2,12] and military aircraft. In addition a special viewing window consisting of germanium, silicon or zincselenide material must be installed for the imager. An infrared thermography system installed in one of the F-18 aircraft of the NASA Dryden Research Center provides a solution to this problem. The infrared thermography system consists of a visible spectrum and thermal imager located in a pod mounted near the lower corner of the port engine inlet, a system controller installed in the rear cockpit, and a Hi-8 video recorder. The imager has a field of view of more than 180° in the horizontal plane and approximately 90° in the vertical plane. By flying in formation with a subject aircraft, detailed images of surface thermal patterns can be obtained.

Although the combination of formation flight and infrared thermography virtually eliminates the problem of limited field of view, it may introduce other problems. First, images may be blurred as a result of a speed difference between the two aircraft and/or as a result of camera motion. This has not been a problem in previous flight experiments with a fixed imager mounted in the fuselage or a wing pod and the imager focused on the surface of the same aircraft. However, it can be a

problem if the infrared system is used remotely to image surface thermal patterns of other aircraft. Second, the orientation between the aircraft carrying the imager and the subject aircraft is variable. Again this has hardly been a problem in previous flight experiments with a fixed imager mounted in the fuselage or a wing pod and the imager focused on the surface of the same aircraft. These and other problems can be solved using digital image enhancement and restoration. Previously very little work has been done to enhance the infrared images obtained in aerodynamic research. An exception is the work by Bouchardy et al.[13] who describe techniques used to process and enhance infrared images. Digital image processing may even eliminate the need for surface treatment to reduce heat conductance within metal structures, thereby eliminating the need for any modifications to the subject aircraft.

In the following section, Dryden's infrared imaging system and the image processing procedure is described in more detail. Next, this procedure is applied to analyze data for a T-34C acquired with the infrared imaging system.

Procedures

In Figure 1, a flow chart depicts the various elements of the in-flight infrared flow visualization method.

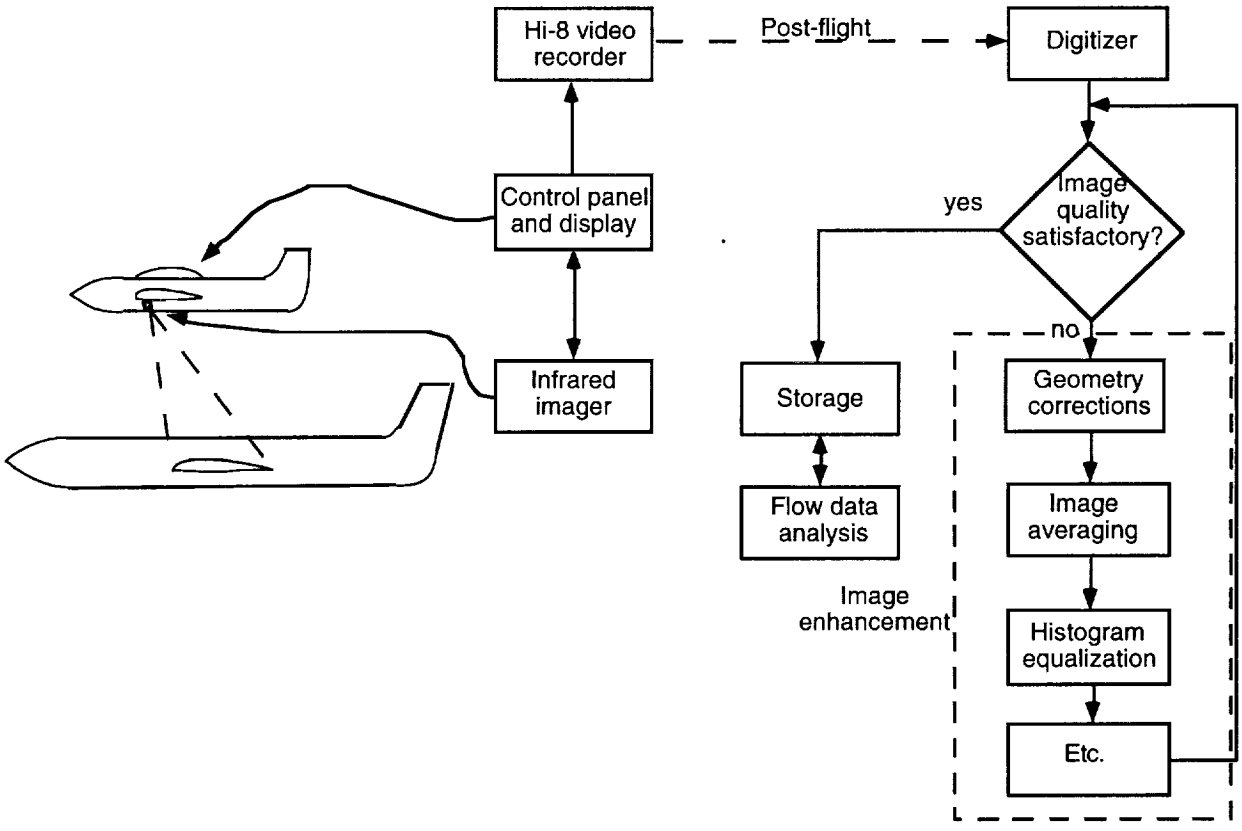

Figure 1. Flow chart depicting various elements of in-flight infrared flow visualization.

- **NASA Dryden's F-18 with infrared imaging system**

As mentioned earlier, the infrared imaging pod is located near the left engine intake of the F-18 (Figure 2a) and the unit's control panel and display are mounted in the aft cockpit. It's field of view is more than 180° in the horizontal plane and approximately 90° in the vertical plane. The infrared imager has the following specifications

image field (2 discrete settings):	3° × 3°
	12° × 12°
spectral sensitivity:	8 - 12 μm
temperature sensitivity:	< 0.1 °F
resolution:	875 lines of resolution

The imager has a target lock feature that largely eliminates the problem of motion blur and was used with some success in the initial flight experiments. When successfully enabled, the lock holds the selected target in the center of the video frame. The target lock is capable of tracking targets with a temperature difference as small as the imager's minimum resolvable temperature.

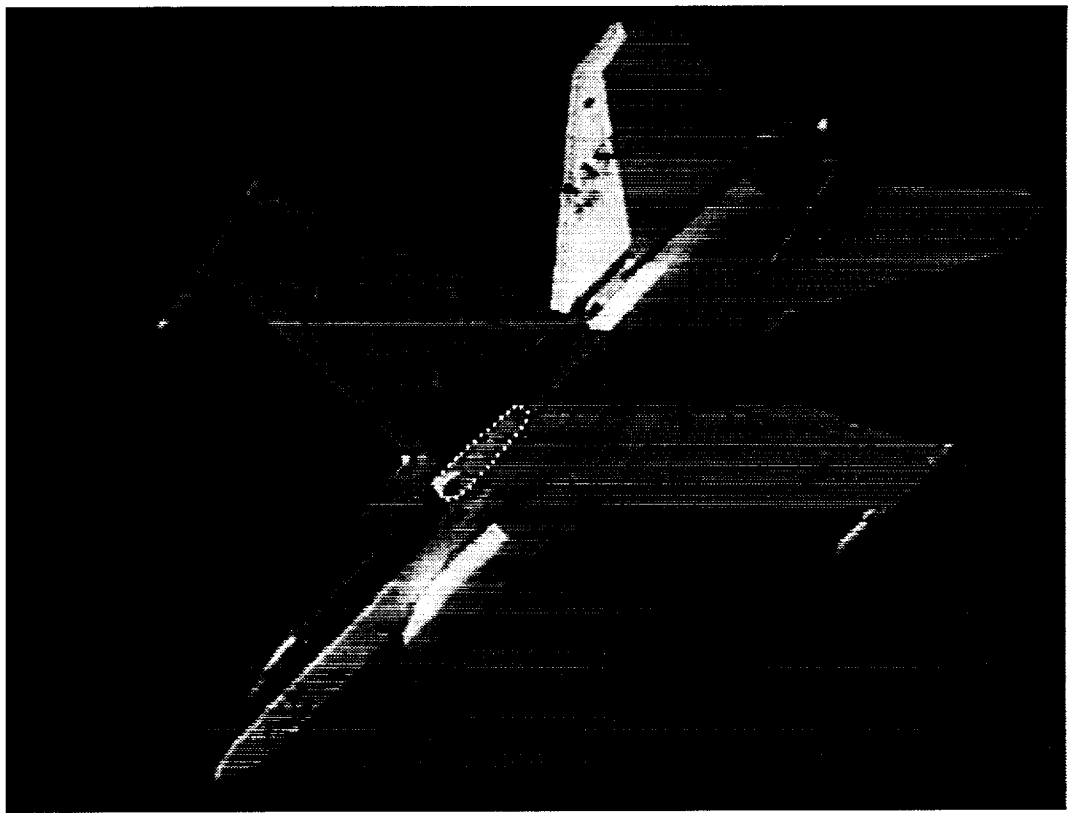

Figure 2a. NASA Dryden's F-18 with infrared imaging system. The pod, indicated with a white outline, is located near the port engine intake.

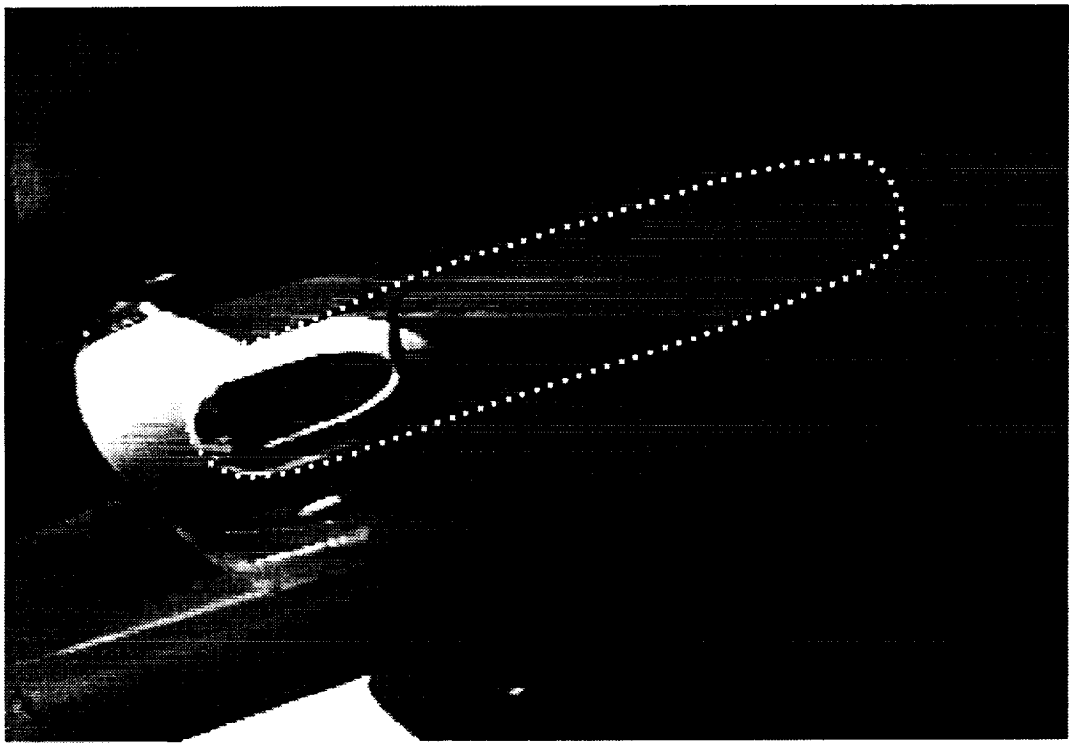

Figure 2b. A close-up of the infrared imaging pod. The pod is outlined in white for clarity.

During the experiment, analog images are recorded on Hi-8 video for post-flight analysis.

After the flight, the video tape is screened and the most significant segments are marked for digitization.

• Image Processing Procedure

The image processing procedure consists of four components:

i. digital acquisition of images,
ii. spatial geometry corrections,
iii. frame averaging, and
iv. image enhancement.

i. Digital acquisition of images

Before any post-processing could be performed, the images had to be transferred from analog Hi-8 videotape to a digital format. The analog to digital transfer used products readily available in the industrial video market. The transfer procedure attempted to preserve image fidelity as much as possible so that even information which was not readily visible remained available for post-processing.

A Sony EVO-9850 Hi-8 editing deck was connected via S-video to a Truevision Targa 2000 CA/V. S-video was preferred over a composite signal because the separation of chrominance and

luminance signals maintains better image fidelity during the transfer.[14] The Targa 2000 CA/V was driven by a Macintosh 9500/150 with 80 MB RAM running Adobe Premiere 4.0.1.

In the case presented in this report, video was captured as a 320x240 Quicktime movie at 30 frames/second using Targa's proprietary hardware codec. Because the digitized video would later be processed on a computer without a Targa system, the Quicktime movie was converted to use no codec (i.e., no compression). Although using no compression greatly increased file size, image fidelity was maintained because no information was lost through a lossy codec (i.e., an image compression scheme which removes data not discernible by the unassisted human visual system).

The Quicktime movie with no codec was transferred to the post-processing system. Individual frames were saved as 8-bit bmp files for image processing.

Future analog to digital transfers will use a different procedure. Instead of capturing a video stream to a Quicktime movie, individual frames will be batch captured to PICT or bmp files. Grabbing individual frames eliminates the need for the lossy Targa codec, thereby maintaining image fidelity during the transfer. Transferring directly to a still image format also expedites the procedure. A deck controller such as the Pipeline Digital ProVTR or Videonics MediaMotion is required for batch capturing. Future captures will also be at a resolution of 640x480.

ii. Spatial geometry corrections

Most digitized frames require some sort of spatial geometry correction to:
- align several images for averaging, and/or
- generate a preferred viewing angle which was not directly available from the original video.

Geometric corrections and all other image processing were performed on a 180 MHz Pentium Pro running MATLAB 5.1.0.421 with version 2.0 of the Image Processing Toolkit.

There are three geometric correction schemes, with varying accuracies, preparation times, and computational times. The schemes can be characterized as follows:

a. assume rotation only in the plane of the image,
b. rubber-sheeting of the 2-D image to another 2-D image,
c. full transform of 2-D image to 3-D space.

a. assume rotation only in the plane of the image
This method is the simplest but also the most limited. Defining the z-axis as perpendicular to the image plane, this method assumes that rotational correction is only necessary about the z-axis. Geometric correction is reduced to rotating, scrolling, and resizing the image.

Only two fiducial marks are required to determine the correction necessary. However, the original footage must be stable enough that rotations about the x-and y-axes can be neglected. Although effective for aligning images, this method cannot project alternate viewing angles.

The effective application of the imaging system's target lock made this method adequate for the case presented in this report. The imaging system locked the round turbulence trip/fiducial mark near the leading edge (see Figure 3) into the center of the frame. The required rotational correction about the z-axis was at most 2.5°. Rotations about the x- and y-axes were small and ignored.

Translation and rotation were performed with MATLAB's image processing toolkit and some custom written scripts. To improve accuracy, three fiducial marks were used instead of two.

b. rubber-sheeting of the 2-D image to another 2-D image
In rubber-sheeting or image-warping, the original image is two-dimensionally stretched into the desired shape as if it were on a sheet of rubber. The image is discretized into a grid by fiducial marks on the subject (in this case, a wing). The grid points are then mapped to corresponding locations at the desired viewing angle. Areas between grid points are mapped over with interpolation.

Rubber-sheeting provides rotational and translational correction in all directions. However, the simple interpolation between grid points does not accurately correct perspective. This method also uses a large number of fiducial marks, requiring more preparation time of the subject and more time during image processing when each mark is manually identified.

c. full transform of 2-D image to 3-D space
The full 2-D to 3-D transform is the most mathematically rigorous and computationally demanding method. A 2-D image and additional information are used to determine the subject's 3-D position. An alternate 2-D view can then be projected. There are at least two approaches; the 2-D image is augmented with either:

- fiducial markers
- known attitudes of the camera and target

Both approaches were used in the Space Shuttle IRIS experiments[15] with limited success. However, the inability to accurately transform the 2-D image was attributed to factors unique to the IRIS experiment (e.g., a defocusing effect in the telescope).

In the IRIS experiment, the outline of the shuttle was used as a fiducial contour. The position of a plane can be determined with six fiducial points, as detailed in Appendix A.

The 2-D to 3-D transform can make rotational and translational corrections in all directions. The 3-D transform also properly corrects perspective. It requires fewer fiducial marks than rubber-sheeting and consequently less manual preparation and processing. It is more computationally intensive than rubber-sheeting, but the 3-D transform should be within reasonable capability of current computers.

This study is currently investigating implementation of a 2-D to 3-D transform based on six fiducial points.

iii. Frame averaging

Temporal averaging improves the signal-to-noise ratio as the square root of the number of frames.

For the image in Figure 3b, 44 frames (including the image depecited in Figure 3a) were averaged together after registration via geometry correction. The signal-to-noise ratio theoretically improved approximately 6.6 times. Note in Figure 3b that boundaries appear cleaner and regions of color are more uniform.

The averaging was performed with a simple MATLAB script.

Figure 3a. Infrared image of T-34C starboard wing. Single frame, 320x240 captured from Hi-8 video. Flow direction from right to left.

Figure 3b. Infrared image of T-34C starboard wing. Average of 44 frames, 320x240 captured from Hi-8 video. Flow direction from right to left.

iv. Image enhancement

Image enhancement is a broad term applying to procedures which make details more discernible to the human visual system. Some enhancement techninques employed in this study are described below.

• *Sharpening*
The averaged images are sharpened to enhance edges. Concentrating edges makes the images easier for the human eye to work with; human vision favors edges over uniform regions.[14]

Figure 3c. Infrared image of T-34C starboard wing. Average of 44 frames, 320x240 captured from Hi-8 video. Unsharp masking was applied to enhance edges. Flow direction from right to left.

Many edge enhancement techniques are available. Figure 3c is the result of the application of unsharp masking to the image in Figure 3b. Note that details register more readily to the eye in the edge enhanced image.

• *Histogram adjustment*
Histogram adjustment changes the distribution of brightness in an image. By manipulating the histogram, even subtle differences in brightness can be made readily visible. Histogram adjustment should be a key tool in visualizing boundary layer transition.

However, as visible in Figure 3a, 3b, 3c, and 3d, horizontal banding in the original video severely limited the effectiveness of histogram manipulation.

• *Pseudocolor*
Pseudocolor is the application of color to represent shades of grey. The human eye can distinguish more colors than grey scale values making pseudocolor a useful tool for studying infrared

images.[14] Pseudocolor, unlike grey scale, is not a continuous function of intensity. It is therefore important to select a pseudocolor map with an adequate number and balanced distribution of colors; poor choice of the pseudocolor map can erroneously emphasize features in an image. In Figure 3d, the previous image is shown in pseudocolor. The 256 grey levels of Figure 3c are mapped to a 256 color spectrum (linear variation of hue, maximum saturation, and intensity).

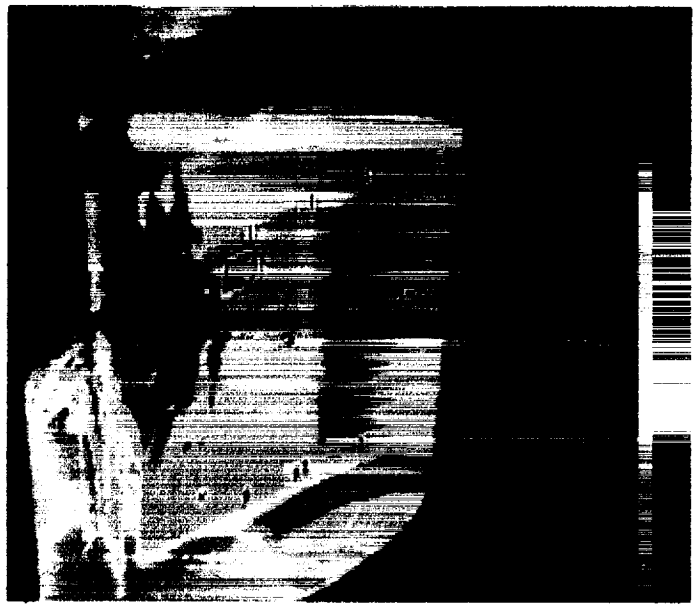

Figure 3d. Infrared image of T-34C starboard wing with pseudocolor applied. Average of 44 frames, 320x240 captured from Hi-8 video. Unsharp masking was applied to enhance edges. Flow direction from right to left. See Figure 3c for greyscale comparison.

Results

A NASA T-34C was used as the subject airplane for the transition experiment. This single-engine turboprop airplane is unpressurized and has a two-place tandem cockpit arrangement. Because the infrared pod is located on the lower port side of the F-18, field-of-view considerations resulted in the selection of the starboard wing of the T-34C as the transition test surface. In Figure 4, the T-34C is shown in top view and the two patches of self-adhesive vinyl which were added in the outboard-wing region are depicted. During the experiment, imager field-of-view requirements forced the F-18 to fly slightly above the T-34C and, consequently, the former was the lead airplane in the two-plane formation. As a result of this test requirement, the available speed range was quite limited. In level formation flight at an altitude of 10,000 ft, a safe lower airspeed limit for the F-18 is approximately 135 KCAS. The maximum airspeed of the T-34C while retaining sufficient maneuverability to stay in level flight formation is approximately 160 KCAS and this dictated the upper limit of the speed range during the test.

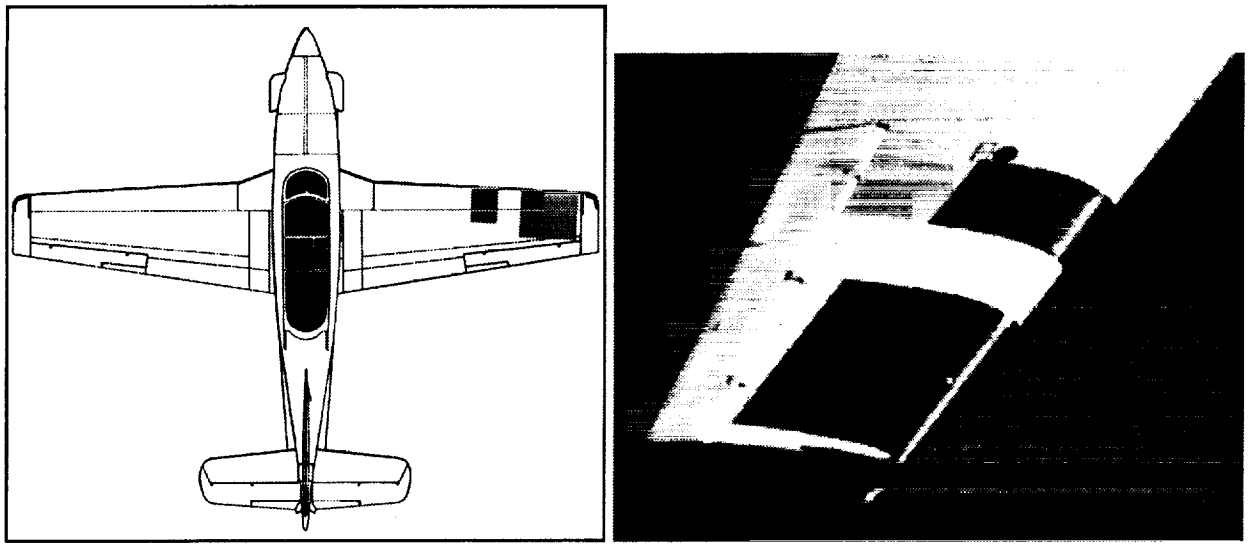

Figure 4. (a) Planview of T-34C.[16] The grey regions on the starboard wing indicate areas where black vinyl sheets were applied. (b) Photograph of the transition test surface on the T-34C starboard wing. Note the black vinyl covering.

Before the experiment, a two-dimensional aerodynamic code was used to predict the transition location at the test conditions. The wing of the T-34C utilizes the NACA 230xx airfoil to provide its section shape with a maximum thickness-to-chord ratio of 0.165 at the root and 0.12 at the tip. In Figure 5, the airplane lift coefficient, C_L, and the Reynolds number, Re, is shown for the T-34C in level flight. Assuming that this lift coefficient is representative of the sectional lift coefficient in the mid-to-outboard region of the wing (a reasonable assumption for an airplane with an unswept, moderately-twisted wing), the aerodynamic code MSES[17] was applied to predict the transition location for the NACA 23012 airfoil at matching lift coefficient and Reynolds number. In Figure 6, the predicted transition location is plotted at a function of calibrated airspeed. The results show that transition is predicted to occur just ahead of the quarter-chord location.

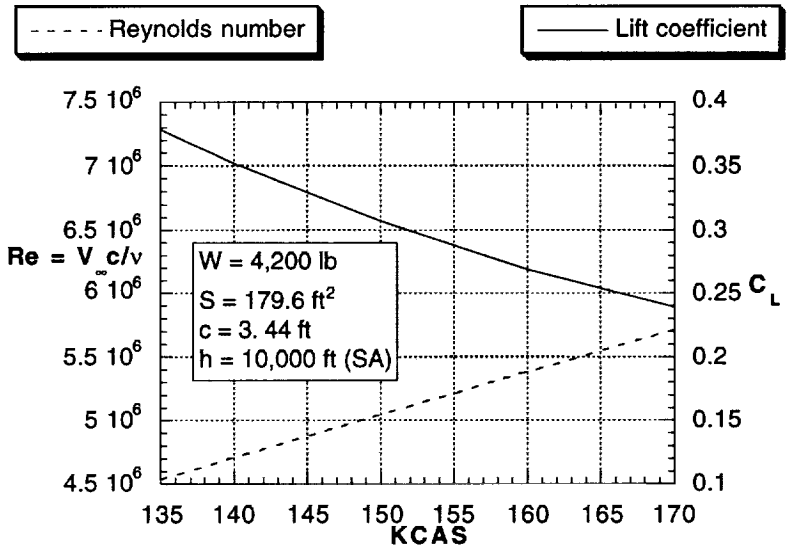

Figure 5. Airplane lift coefficient and Reynolds number for T-34C in level flight.

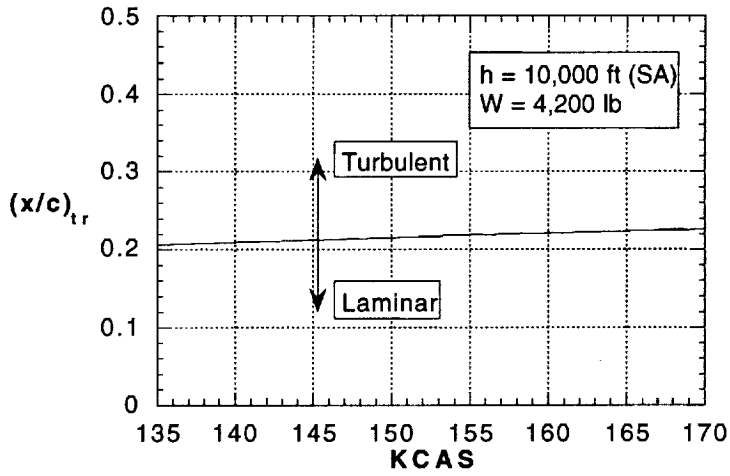

Figure 6. Predicted transition location on upper surface of T-34C wing in level flight.

The thermograms indicate transition at 21% chord. This value correlates well with the predicted transition location. The two sets of double black marks (aluminum tape applied on top of the outboard vinyl sheet) in Figure 7 were located on top of the front spar at the 25% chord location. The single black marks are 6 inches upstream and downstream of the 25% chord location. In Figure 7, the inboard vinyl sheet is also partially visible. The light colored region (i.e., warmer surface temperature as explained earlier) near the leading edge indicates laminar flow and it extends until just ahead of the double black marks; i.e., the 25% chord location. Note that the transition location is also clearly visible on the inboard vinyl sheet. The banding problem prevented detailed analysis of the thermograms to detect the transition location on the untreated metal surface between the two areas covered with vinyl. Clearly visible is the turbulent wedge created by the trip located in the leading-edge region of the outboard vinyl sheet. The light colored region in the aft-portion of the wing is caused by reflections from the bare metal surface.

Conclusions and Recommendations

The results presented in this report prove the feasibility of remote infrared thermography of aircraft surfaces during flight to visualize the extent of laminar flow on aircraft. In general, it was determined that such thermograms can be taken successfully using NASA Dryden's F-18 with the infrared imaging system and that the transition pattern and, thus, the extent of laminar flow can be extracted from these thermograms. Depending on the in-flight distance between the F-18 and the target aircraft, the thermograms can have a spatial resolution of as little as 0.1 inches. The field of view provided by the present remote system is superior to that of prior stationary infrared thermography systems mounted in the fuselage or vertical tail of a target aircraft.

An image processing procedure was developed which improves the signal-to-noise ratio of the thermograms. Problems encountered during the analog recording of the thermograms (banding of video images) made it impossible to evaluate the adequacy of the present imaging system and image processing procedure to detect transition on metal surfaces. The high reflectance, high thermal difussivity, and low emittance of metal surfaces tend to degrade the images to an extent that

makes it very difficult to extract transition information from them. The application of a thin (0.005 inches) self-adhesive insulating film to the surface is shown to solve this problem satisfactorily.

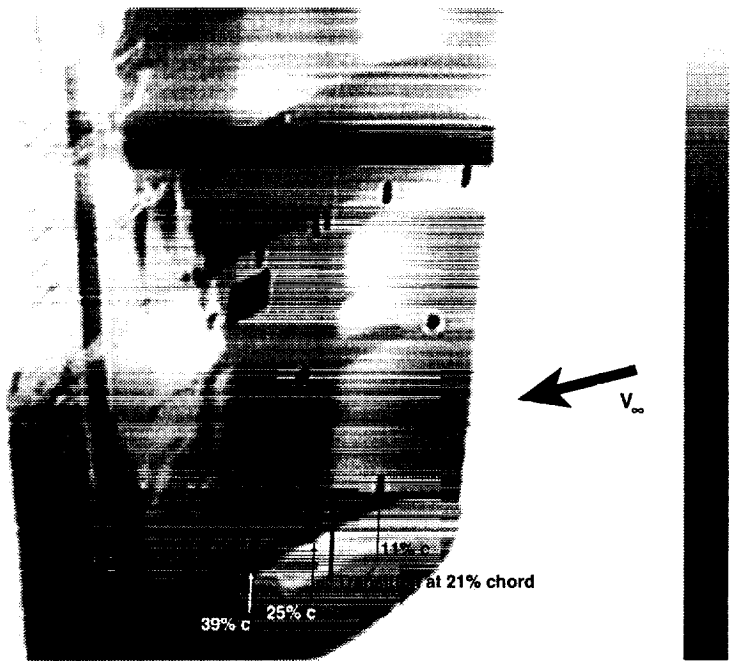

Figure 7. Thermogram showing the boundary layer transition pattern in the outboard wing region of the T-34C.

The infrared imaging system has been upgraded since the initial visualization flights with the T-34C. It is proposed to redo the T-34C experiment to evaluate the improvements made to the infrared imaging system. Following flight experiments may target the Lockheed L-1011 with the high-lift system retracted and extended; the L-1011 is a good example of a large civil transport airplane. The feasibility of laminar flow on the L-1011 is discussed in Appendix B. Another suitable target airplane may be a Cessna Citation, a good example of a low-drag business jet. Citations are designed to have extended runs of laminar flow on their wings in cruise. Application of the remote imaging system and the image processing procedure to evaluate the flow phenomena for a wide range of airplanes will provide a better understanding of the strengths and weaknesses of this test technique.

Appendix A

Camera Calibration Method for Image Geometry Correction

Green et al.[15] describe two different techniques to transform infrared image information to actual physical locations on the space shuttle surface. The first technique, the so-called computer graphics method, is based on the manual manipulation (rotation, translation, scaling) of the known shuttle geometry until it matches the edges of the image. Next, the inverse of the resulting transformation matrix is applied to the image pixel coordinates to map them to those of the space shuttle. The second technique, the so-called analytical registration method, is more rigorous but requires knowledge of flight orientation angles for both the target vehicle and the imager vehicle. Here we propose a technique which is similar to the former but here the imager itself is used as a measuring device. Consequently, no detailed information of flight orientation angles is required. This technique, the so-called camera calibration technique, only requires a set of image points whose world coordinates (i.e., body-fixed coordinate system of subject airplane) are known. The derivation of the camera calibration procedure is described by Gonzalez & Wintz[18]. The technique is based on the following set of equations:

$$a_{11}X + a_{12}Y + a_{13}Z - a_{41}xX - a_{42}xY - a_{43}xZ - a_{44}x + a_{14} = 0$$

$$a_{21}X + a_{22}Y + a_{23}Z - a_{41}yX - a_{42}yY - a_{43}yZ - a_{44}y + a_{24} = 0$$

where X, Y, Z represent the coordinates in the global system and x, y represent the coordinates in the image. The calibration procedure requires at least 6 points in the global coordinate system with coordinates (X_i, Y_i, Z_i), $i = 1, 2, ..., m$ and $m \geq 6$. Next, image these points and determine the locations (x_i, y_i) of the corresponding points in the image coordinate system. Last, solve the above system of equations for the 12 unknown coefficients a_{11}, a_{12}, a_{13}, a_{41}, a_{42}, a_{43}, a_{44}, a_{14}, a_{21}, a_{22}, a_{23}, a_{24}. Now, for a given point (X_p, Y_p, X_p) in the global coordinate system we can calculate its location (x_p, y_p) in the image from the above equations. Its value can be determined using bilinear interpolation based on the values of the surrounding pixels. The final step involves plotting this information in e.g. a planform view of the target wing.

Appendix B

Prediction of the Attachment-Line Reynolds Number for L-1011

Future experiments using remote infrared thermography may be conducted using a Lockheed L-1011 as the subject airplane. Transition of the attachment-line boundary layer may cause the flow over the entire wing to become turbulent. Poll[19] claims that the majority of civil aircraft, including the L-1011, will have turbulent attachment lines in cruising flight and that subsequent relaminarization of the boundary layer in regions of favorable pressure gradients is unlikely. However, recent experiments on the B737-100[6,10] have shown that laminar attachment-line flow is not uncommon for civil aircraft and that relaminarization is likely to occur for the wing in the high-lift configuration.

An important parameter when studying the transition characteristics of the attachment-line boundary layer is the attachment-line Reynolds number, $R_{bar} = W_\infty \kappa/\nu$, where $W_\infty = V_\infty \sin\Lambda$ is the spanwise component of the freestream velocity, and $\kappa = (\nu/U_n')^{0.5}$ is the characteristic length. The quantity, U_n', represents the inviscid velocity gradient at the attachment line in the direction normal to it. Various studies, including Ref. 19, have shown that for $R_{bar} < 245$, the attachment-line boundary layer will tend to remain laminar, and turbulent contamination introduced in the boundary layer by significant surface roughness and intersecting turbulent shear layers decays. For $R_{bar} > 245$, the turbulence self-sustains, causing the attachment-line flow, as well as the flow downstream of the attachment line, to become turbulent. In the absence of any contamination, the attachment line remains laminar, and viscous instability followed by rapid transition occurs only if $R_{bar} > 580$.

Assuming that the leading-edge of a wing can be represented by an infinite swept cylinder the following expression can be derived for the attachment-line Reynolds number:[19]

$$R_{bar} = \sqrt{\frac{W_\infty r}{\upsilon} \times \frac{\tan\Lambda}{2}}$$

where r represents the leading-edge radius and Λ the leading-edge sweep angle. In Figure B1 the resulting values for R_{bar} are shown for the L-1011 in steady level flight in a standard atmosphere at a typical weight of 418,000 lb. What becomes clear from these results is that R_{bar} falls below 245 outboard of the engine nacelle for a wide range of feasible flight conditions. Moreover, if the critical level is increased to $R_{bar} = 300$ (attachment-line Reynolds number below which no attachment-line contamination was measured in the aforementioned B737-100 flight experiment nor in the A310-300 flight experiment[20]) then the likelihood of extended runs of laminar flow in the outboard region of the L-1011 wing increases even more.

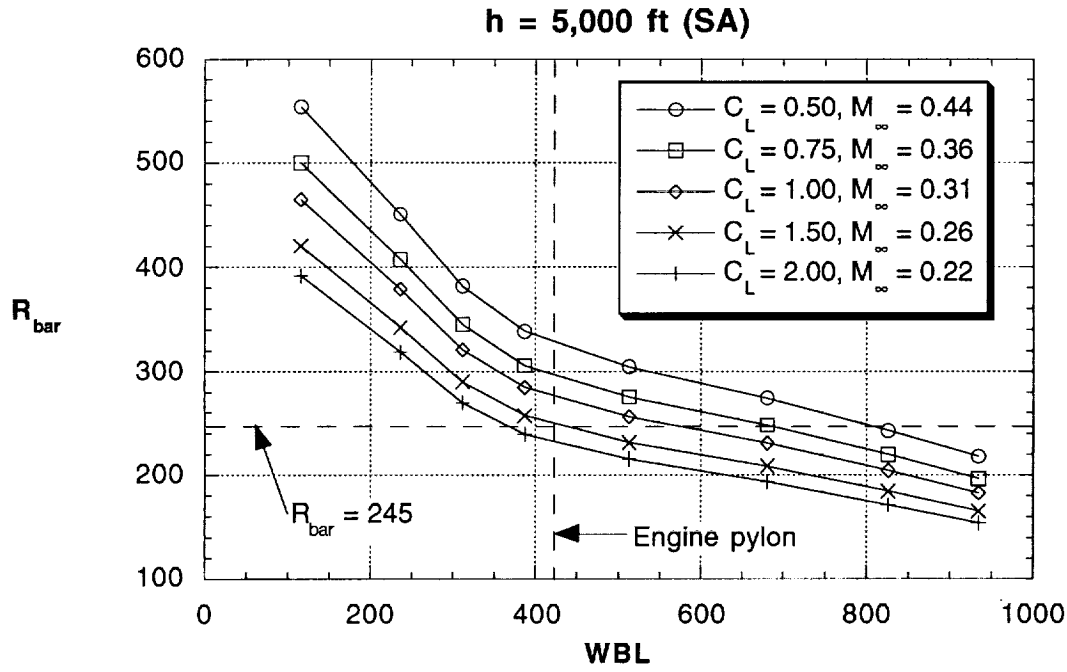
h = 5,000 ft (SA)
R_{bar}
600
500
400
300
200
100
0
200
400
600
800
1000
WBL
C_L = 0.50, M_∞ = 0.44
C_L = 0.75, M_∞ = 0.36
C_L = 1.00, M_∞ = 0.31
C_L = 1.50, M_∞ = 0.26
C_L = 2.00, M_∞ = 0.22
R_{bar} = 245
Engine pylon

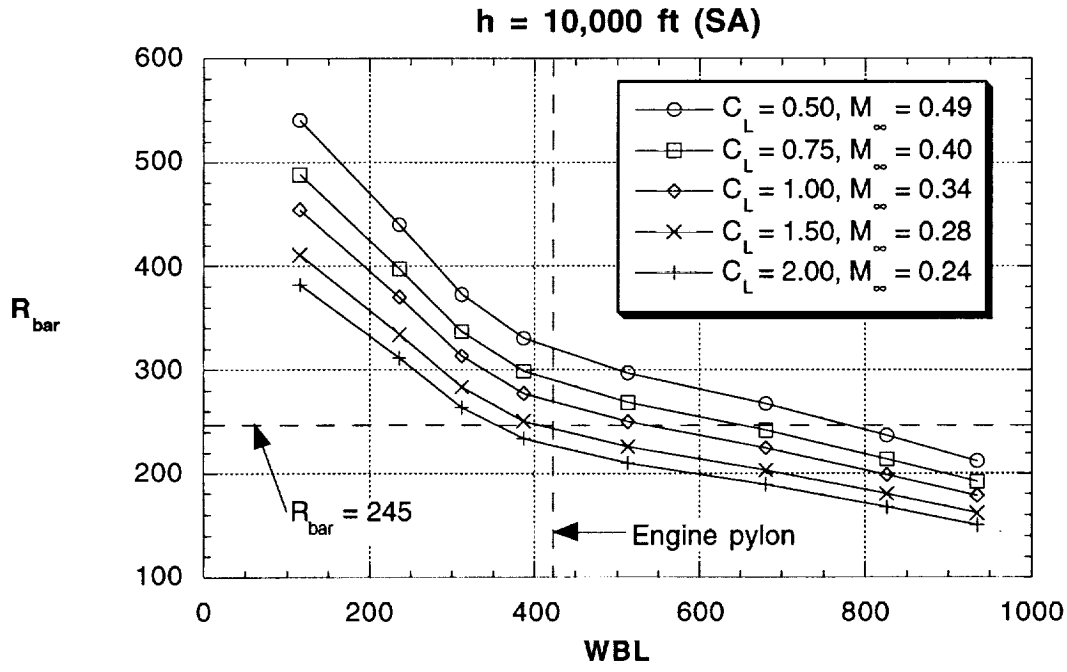
h = 10,000 ft (SA)
R_{bar}
600
500
400
300
200
100
0
200
400
600
800
1000
WBL
C_L = 0.50, M_∞ = 0.49
C_L = 0.75, M_∞ = 0.40
C_L = 1.00, M_∞ = 0.34
C_L = 1.50, M_∞ = 0.28
C_L = 2.00, M_∞ = 0.24
R_{bar} = 245
Engine pylon

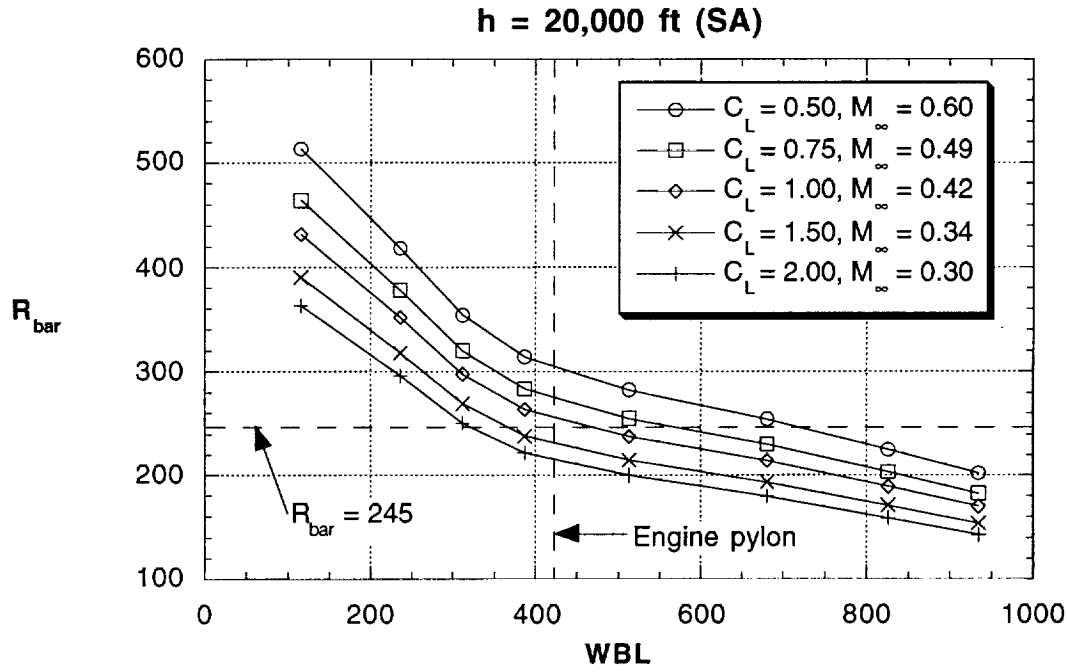

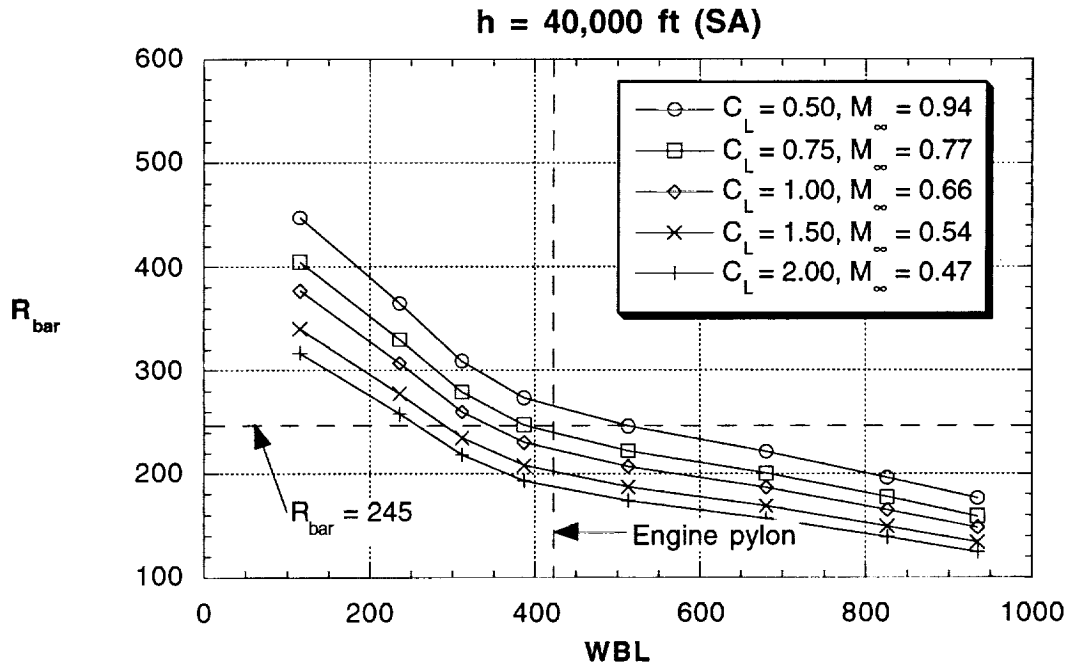

Figure B1. Predicted attachment-line Reynolds number for L-1011 in steady level flight (W = 418,000 lb, Standard Atmosphere).

References

[1] Holmes, B.J., Obara, C.J., and Yip, L.P., "Natural Laminar Flow Experiments on Modern Airplane Surfaces," NASA TP 2256, June 1984.

[2] Quast, A., "Detection of Transition by Infrared Image Technique," *Proceedings of the ICIASF Record*, Williamsburg, VA, June 22-25, Institute of Electrical and Electronics Engineers, New York, 1987, pp. 125-134.

[3] Hall, R.M., Obara, C.J., Carraway, D.L., Johnson, C.B., Wright, R.E., Jr., Covell, P.F., and Azzazy, M., "Comparisons of Boundary-Layer Transition Measurement Techniques at Supersonic Mach Numbers," AIAA Journal, Vol. 29, No. 6, June 1991, pp. 865-879.

[4] Cattafesta, L.N., III and Moore, J.G., "Transition Detection in High-Speed Flows with Luminescent Temperature-Sensitive Paint," Flow Visualization VII, J. Crowder (Ed.), Begell House, pp. 944-949.

[5] Kennelly, R.A., Jr., Westphal, R.V., Mateer, G.G., and Seelen, J., "Surface Oil Film Interferometry on a Swept Wing Model in Supersonic Flow," Flow Visualization VII, J. Crowder (Ed.), Begell House, pp. 302-307.

[6] Yip, L.P., van Dam, C.P., Whitehead, J.H., Hardin, J.D., Miley, S.J., Potter, R.C., Bertelrud, A., Edge, D.D., and Willard, P.E., "The NASA B737-100 High-Lift Program - Measurements and Computations," The Aeronautical Journal, Vol. 99, No. 989, November 1995, pp. 372-386.

[7] Greff, E., "In-Flight Measurement of Static Pressures and Boundary-Layer State with Integrated Sensors," Journal of Aircraft, Vol. 28, No. 5, May 1991, pp. 289-299.

[8] Yip, L.P., Vijgen, P.M.H.W., Hardin, J.D, and van Dam, C.P., "In-Flight Pressure Measurements on a Subsonic Transport High-Lift Wing Section," Journal of Aircraft, Vol. 32, No. 3, May - June 1995, pp. 529-538.

[9] Horstmann, K.H., Redeker, G., Quast, A., Dreßler, U., and Bieler, H., "Flight Tests with a Natural Laminar Flow Glove on a Transport Aircraft," AIAA Paper 90-3044-CP, 1990.

[10] Miley, S.J., van Dam, C.P., Yip, L.P., Willard, P.E., Crowder, J.P., and Wazlavick, R.L., "Slat Transition Characteristics on the NASA B737-100 Aircraft using Infrared Imaging and Hot-Film Anemometry," Flow Visualization VII, J. Crowder (Ed.), Begell House, pp. 950-956.

[11] Henninger, J.H., "Solar Absorptance and Thermal Emittance of Some Common Spacecraft Thermal-Control Coatings," NASA RP 1121, 1984.

[12] Brandon, J.M., Manuel, G.S., Wright, R.E., and Holmes, B.J., "In-Flight Flow Visualization Using Infrared Imaging," Journal of Aircraft, Vol. 27, July 1990, pp. 612-618.

[13] Bouchardy, A.M., Durand, G., and Gauffre, G., "Processing of Infrared Thermal Images for Aerodynamic Research," *Proceedings of SPIE - The International Society for Optical Engineering*, Vol. 397, A. Oosterlinck and A.G. Tescher (Eds.), Geneva, Switzerland, April 19-22, 1983, pp. 304-309.

[14] Russ, J.C., The Image Processing Handbook, 2nd Ed., CRC Press, 1995.

[15] Green, M.J., Budnik, M.P., Yang, L., and Chiasson, M.P., "Supporting Flight-Data Analysis for Space-Shuttle Orbiter Experiments at NASA Ames Research Center," NASA TM 84345, April 1983.

[16] Taylor, John W. R. (Ed.), Janes's All the World's Aircraft, 1989-90, Jane's Information Group Limited, 1989.

[17] Drela, M., "Newton Solution of Coupled Viscous/Inviscid Multielement Airfoil Flows," AIAA Paper 90-1470, June 1990.

[18] Gonzalez, R.C. and Wintz, P., Digital Image Processing, 2nd Ed., Addison-Wesley Publishing Comp., 1987.

[19] Poll, D.I.A., "Transition in the Infinite Swept Attachment Line Boundary Layer," The Aeronautical Quarterly, Vol. 30, Nov. 1979, pp. 607-629.

[20] Thibert, J.J. , "The Garteur High Lift Research Programme," *High-Lift System Aerodynamics*, AGARD CP-515, Sept. 1993, pp. 16-1 to 16-21.